# Current, concentration and overpotential distributions on columnar structured electrodes in a 2-D fuel cell model.

C.F. Zinola*

*Electrochemical Engineering Group, Universidad de la República, J.E. Rodó 1843, C.P. 11100, Montevideo, Uruguay.*
**corresponding author:fzinola@fcien.edu.uy*

**Abstract**

The complete optimization of fuel cell´s performance involves the prediction of its operation conditions and electrochemical characteristics for short and long-time periods. One of the topics not studied in detail is the change in the surface morphology of metallic catalytic layers as a time-dependent function of the fuel cell working conditions. For single platinum catalysts a columnar growth is demonstrated after 1 month of hydrogen/oxygen continuous operation at the *plateau*, where electrochemical distributions of smooth surfaces are not operative. Since they act as a completely dynamic system, numerical solutions are not useful as they permanently need parametric profile optimizations. The employ of exact analytical functions instead, reduces large computational times and assures this information only knowing the final structure morphology. In this sense we encouraged current, concentration and potential shapes for these columnar electrodes adapting mass balance differential equations with a parametric profile to model these columns (trochoid curvilinear contours). The analytical solutions were compared with those of a smooth surface (early uses of the fuel cell) and with experimental values obtained using a home-made hydrogen/oxygen polymeric membrane cell.

## 1.- Introduction.

Green hydrogen, obtained from polymer electrolyte electrolysers, is taken now as the new energy vector revolution and when converted with fuel cell devices, zero emission energy in high efficiency powers is settled for static, transport and industrial applications [1-3].

However, some technological problems still need to be solved and studied. Thus, long-time operation polymer electrolyte (PEM) fuel cells exhibit unexpected roughening even under low current operation ranges. Besides the analysis in membranes water contents, heat losses, temperature and pressure constancies, the stability of anode and cathode catalyst layers are one of the topics not studied in detail as necessary. Moreover, in some cases uncontrolled growth establishes short-circuiting between cathode and anode making the entire stack collapsing [4, 5].

Most of the catalyst layers consist of platinum-group alloys on carbon supported bases, which during operation start to grow with different morphologies and geometries. In the case of carbon supported platinum electrocatalysts, columnar structured ensembles get rise with defined structures and surface roughness. While the fuel cell works platinum ions´ dissolution occurs and depending on the electric potential redeposition gradually develops to certain sites yielding preferred crystallographic orientations in fractal structures categorised as self-refined or self-similar ordered anisotropic ensembles. These electrodes behave as rough polycrystalline platinum that are stable for long time operation periods even at large anodic potentials with roughness up-ranging to $10^{3-4}$ [6, 7].

Kulikovsky made several approaches to model and explain the current density distribution with analytical and numerical solutions on 2D and pseudo 1D fuel cells along a channel [8,9] and on the catalyst layer [10, 11]. They were based on the description of the oxygen mass transport from the cathode catalytic layer, charge transfer from the Nafion membrane to the catalytic layer and the electrode kinetics of the oxygen reduction itself.

Maybe the most interesting innovation, with good results, is the employ of a pseudo 2D domain (or 1D + 1D model) were the equations of those transports in the catalytic layers, gas diffusion layers and membrane interfaces are described solely in the direction of the gas flux entrances parallel to them. Those pseudo 2D models were previously used by Maranzana *et al*. [12], Mainka *et al.* [13] and Chevalier *et al.* [14] with the advantage of simplifying these differential equations giving rise to a much more generalizable and descriptive analytical exact solutions.

Literature reports the employment of dimensionless numbers in fuel cell engineering for the variety of the PEM fuel cell models. Gyenge [15] published a comprehensive review of all dimensionless numbers, some of them repetitive or redundant, but a list of no less than 25 was found. Chevalier [16] solved the system of the fuel cell introducing with the Pi theorem only 3 dimensionless numbers with a good characterization under 4 distinct regimes. Xuan *et al.* [17] centred their study on the application of Damkhoeler, **Da**, Peclet, **Pe**, and Wagner, **Wa**, numbers since they have the advantage to allow the comparison between the performances of different configuration of fuel cells regardless the operating conditions or materials. Their main impact can be seen in the power density curves, however all of them are defined for 1 D variable dependences.

Maybe the first mathematical treatment to solve the mass transport limitations for oxygen reduction in PEM fuel cells was that of the Perry and Newman method [18].Two mathematical models of gas diffusion layers were investigated. The change in the Tafel slope due to flooded porous electrodes (to a value twice the original) was studied there solving a non- uniform current distribution because of ohmic losses, either from the electrolyte or the solid matrix. However, the differential equation for mass transport coupled with electrode kinetics was evaluated for spherical coordinates considered the Thiele´s modulus similar to [19]. They considered the electrodes as sphere configurations of carbon/platinum ensembles embedded in the three phase arrangement.

Exact analytical solutions have been faintly encouraged since most of the differential equations cannot been solved using classical mathematical procedures. In this sense, Chevalier *et al.* [16] consider a combination of combination of 3 equations. The first one is oxygen mass balance in the channel assumed to be a plug-flow with an averaged velocity in a single 1 D direction. The second is the classical dependence of current density on the concentration gradient in the gas diffusion layer in the other direction. However, the third, at a plane cathodic catalyst layer of the electrochemical reaction takes place homogeneously throughout its thickness modelled by a 1 D mass transport Tafel law. The exact solution were found for 4 cases to reduce the complexity of the equations.

On the other hand, the treatment of a two-dimensional model for oxygen mass transport in a gas diffusion layer of a PEM cell has been simplified into a pure diffusion situation introducing an equivalent oxygen diffusivity [20]. The rate of the electrochemical reaction within the catalyst layer was again simplified to provide a mass transfer modified Tafel equation, but introducing a water electroosmotic drag coefficient, Stefan-Maxwell

interdiffusions and a Bruggeman´s porosity factor. For the two-dimensional Laplace's equation of mass transport they used the adequate boundary conditions in distinct zones of the diffusion thickness discretized to apply the finite difference method and solved using an alternating-direction explicit method. The concentration and current distribution for various operating conditions showed that the gas diffusion layer thickness should be as thin as possible if the associated porosity is low.

Moreover, the problem of using a proper oxygen velocity has been also encouraged by Chevalier *et al.* [21] using electrochemical impedance. They used a time dependent 1 D coordinate approach under potentiostatic conditions, that is, constant overpotential, deriving an analytical expression of the channel impedance at low frequencies, which was a function of channel geometry and air velocity only. The comparison between theoretical air velocities obtained from mass flow were fewer than 13% of error with results measured on the fuel cell impedance at current densities less than 0.42 A $cm^{-2}$.

Therefore, we propose a transformation of the 2 D mass transfer differential equation into a single curvilinear variable expression to solve it using common initial and contour conditions and predict the electrochemical behaviour of the PEM fuel cell with columnar structured electrodes.

## 2.- Experimental Results

### 2.1. Development of Surface Roughness as Columnar Platinum Surfaces.

The changes in the morphologies of the anode and cathode catalyst layers were followed voltammetrically as a function of time with parallel experiments disassembling the fuel cell and approaching a platinum large area electrode as auxiliary and a fine capillary normal hydrogen electrode as reference. For this purpose a thin layer cell was used using deoxygenated 0.5 M sulphuric acid as supporting electrolyte. A clear difference between the initial cathodic and anodic surfaces was obtained using large platinum loads (*i.e*. higher than 3 mg $cm^{-2}$) and after 1 month of full operation at 0.96 V (ca. 0.1 A $cm^{-2}$). For lower loads it was possible to see similar responses in the cyclic voltammetric results but after larger operation times where the potential and current density´s oscillations were higher than 20 %. The most noticeable electrode upon this transformation was the cathode.

Figure 1 (I) shows the initial cyclic voltammetric response of cathodic platinum layer supported on carbon Vulcan XC of 3.6 mg $cm^{-2}$ between 0.020 and 1.50 V run at 0.010 $Vs^{-1}$ in 0.50 M sulphuric acid. The voltammetric profile resembles closely that of a large-area polycrystalline surface with some ohmic drop caused by the presence of carbon basement. Moreover, the ratio between the current intensity of the weakly adsorbed hydrogen, (110) stepped planes, and the strongly adsorbed hydrogen, (100) stepped planes, is about 100 % higher than that of smooth platinum surface. Figure 1 (II) depicts the equivalent response of the cathode after 1 month of full and continue operation. It has to be said that some oscillations occur in the potential developed by the hydrogen fuel cell, that is, 0.90 to 0.96 V and also on the temperature (from 55 to 65 $^{o}$C) and current densities (from 0.07 to 0.1 A $cm^{-2}$). The most importance difference in this response is the decrease in the ohmic drop contribution, surely due to the growth of more ordered columnar structure. Moreover, a hump is seen along the double-layer region, that is, near 0.55 V which is typical of long range ordered (111) stepped surfaces or water ensemble adsorption contributions. Finally, the higher contribution of the peak for platinum oxide formation at 1.05 V is further evidence that

columnar platinum is as stable as bright polycrystalline surfaces. The calculation of the surface roughness considering the full-monolayer premise yields a value of about 50 using the carbon monoxide oxidative desorption method [22]. The electrochemical response of the columnar platinum electrode was also described in another paper but for carbon-less electrodes [23]. The *ex situ* STM images are also shown in the topographic mode (Figure 2) to calculate the mean separation and height of the platinum columns. For this purpose it was also required some scanned images on the 2 coordinates to be calculate these values more properly as detailed below.

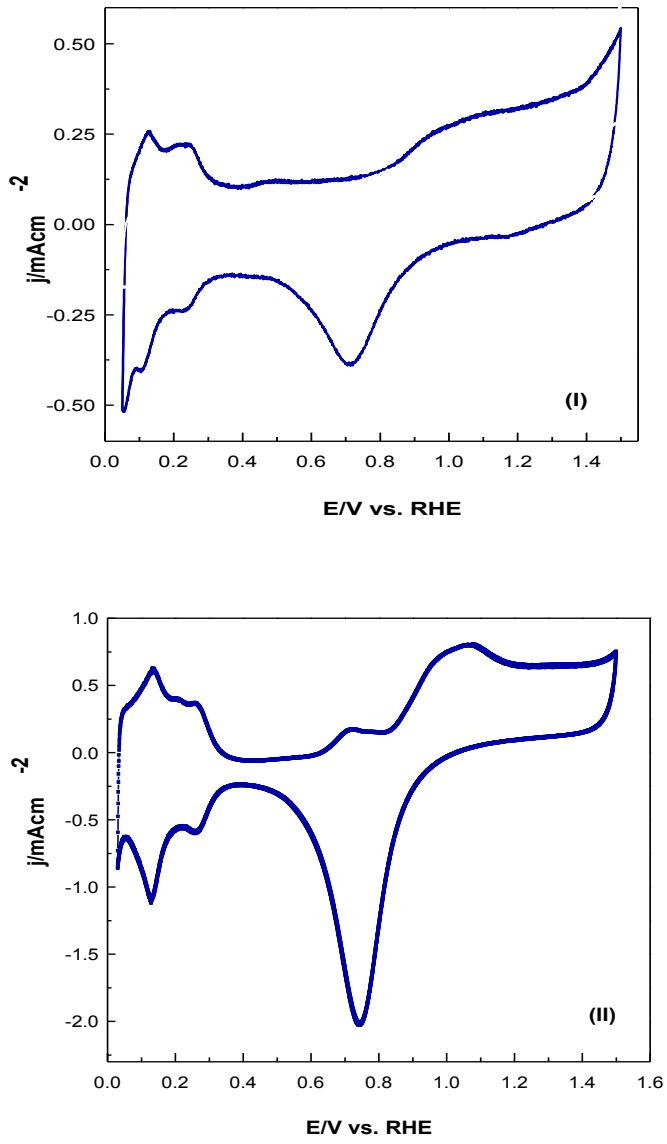


**Figure 1.-** Initial cyclic voltammetry (I) and final (II) profile for the cathodic catalytic layer after 1 month of continuous fuel cell operation at the *plateau*. Cyclic voltammograms were run between 0.02 V and 1.50 V at v=0.010 $Vs^{-1}$ in oxygen-free 0.50 M sulphuric acid at 298 K on the carbon supported catalytic layer.

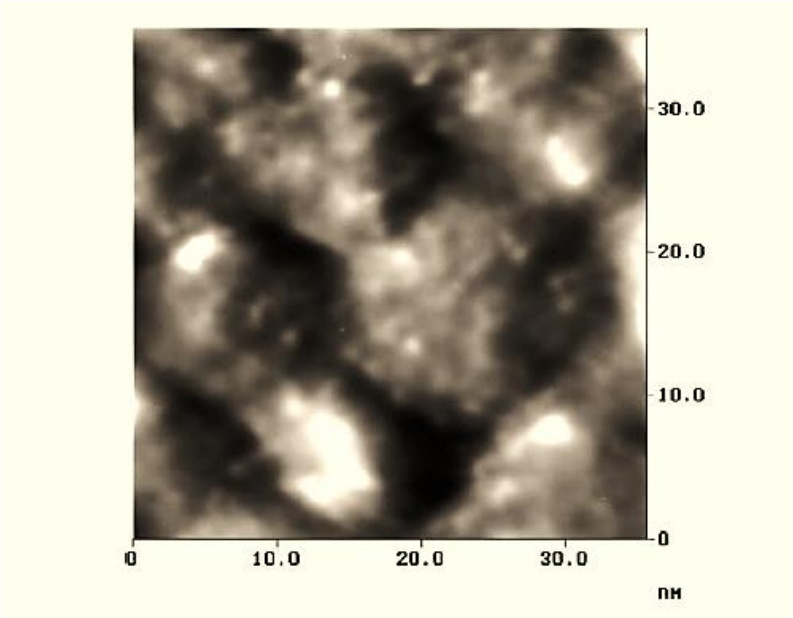


**Figure 2.-** *Ex situ* STM image in the topographic mode for a columnar structure platinum electrode of a 1 month operating hydrogen/oxygen fuel cell.

**3.- Theoretical Considerations.**

As it has been reported before [7] a fractal distribution can be used to describe the electrochemical growth of a platinum surface of large roughness. However, at this scale of transformation the anisotropic growth at this columnar profile (self-affine fractality) has a little evolution, so no dynamic scaling was possible. To envisage the physicochemical properties at this type of surfaces, we have shown [7] that the consideration of curvilinear periodic curves (as trochoids or cycloids) are useful, *i.e.* points in a plane running along a single line direction defined with parametric planar trigonometric functions. Thus, we will use them here too but changing the mass balance equation with the input of electrode reactions.

The obtained columnar surface after a 1 month of full operation at the *plateau* of the PEM hydrogen/oxygen fuel cell is characterised by $\lambda$ = 0.5 and $\alpha$=0.5 (Figure 3). The height and width of the columns calculated from STM measurements (*ex situ* STM top and cross sectional snapshots) were 1500 to 2000 and 15 nm, respectively. However the distance from one column to the other was rather stochastic aprox. 20 nm, but after relaxation it reduces to less than 10 % of this value. Moreover, it was found that the expected cylindrical morphology was really a truncated smooth curved cylinder.

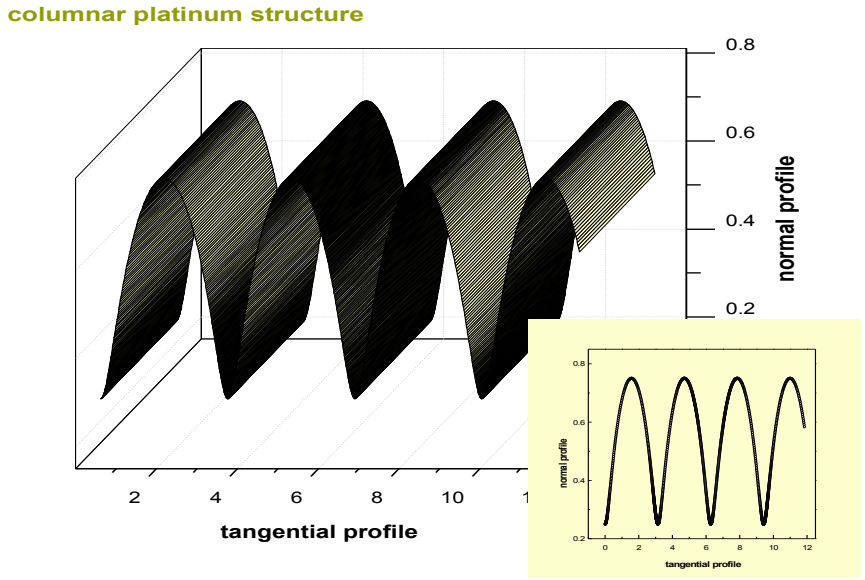


**Figure 3.-** Parametric representation of the growth of a periodic columnar surface (trochoid or shortened cycloid) of a platinum cathodic electrode after 1 month of fuel cell operation. $\lambda$=0.5, $\alpha$=0.5 (continuous line).

There are very few studies using a 2 D model for fuel cells proposing exact analytical functions from mass and linear momentum balances coupled with electrochemical reactions. Since the rate determining step is the oxygen mass transport, the focus is put mostly on it on this channel and diffusion layer together with the charge transport in the catalytic layer due to the cathodic reaction. Moreover, most of the discussion arose from the morphology of the platinum surface at the catalyst layer, either smooth or isotropically uniform rough columnar shape. Using the mass transfer modified Tafel law we will calculate the overpotential profile in parallel to further find the polarization curves.

**3.1.- Generalities on a two dimensional approach.**

As a first consideration we can say that when the reactant (oxygen) is relatively far from the surface, a microprofile describes very well the hydrodynamics of the system (Figure 4). The convective diffusion layer is much larger than the height of the column and therefore, the full developed stream has to be $\mathbf{U^o}$.

$$v_x\left(\frac{\partial C}{\partial x}\right)+v_y\left(\frac{\partial C}{\partial y}\right)=D\left(\frac{\partial^2 C}{\partial y^2}\right) \qquad [1]$$

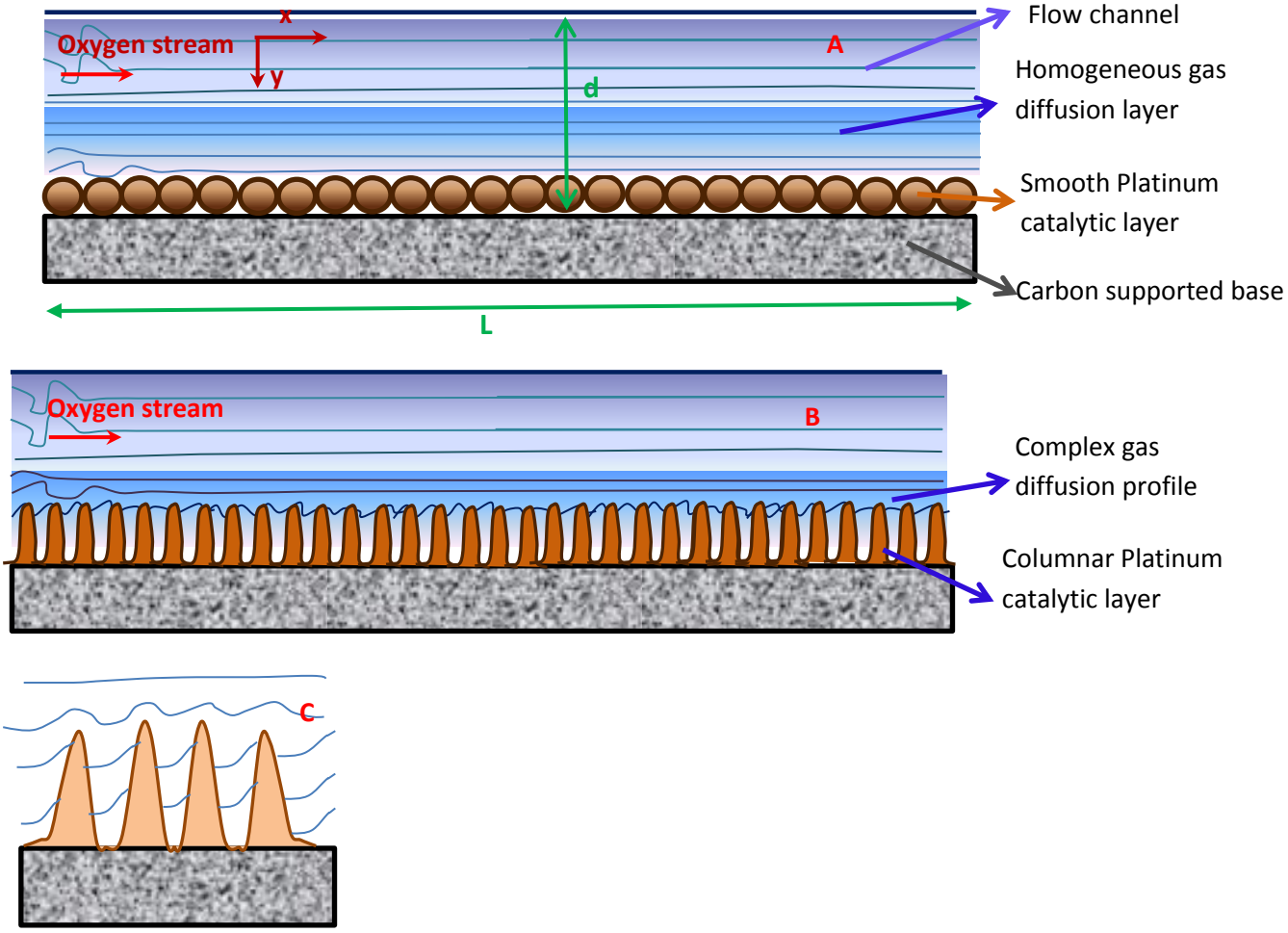


**Figure 4.-** Oxygen flow stream along the cathodic channel of a 2D fuel cell. Steady state laminar convective diffusion under a linear semi-infinite flow. (a) Thin catalytic layer of smooth platinum ensembles. (b) Thin catalytic layer of columnar and regular platinum ensembles. (c) Inset of the columnar electrode with the flow stream velocity evolution.

When the fuel cell is operating, the electrochemical reactions consume reactants between the anode and cathode producing water. Thus, we need to add a gradient of a source term arising from water formation or reactant consumptions. The changes are only on *x* (as the reactants mostly flow along this coordinate) but the current appears normally to it, that is, between anode and cathode at a given *y*.

$$v_x\left(\frac{\partial C}{\partial x}\right)+v_y\left(\frac{\partial C}{\partial y}\right)=D\left(\frac{\partial^2 C}{\partial y^2}\right)\pm\frac{\partial}{\partial x}\left(\frac{j}{nF}\right) \qquad [2]$$

Instead of using the mass corrected Butler-Volmer equation (with overpotential unknown dependence with concentration) it would be better to convert the current density to concentration to have a single and unique unknown function.

$$v_x\left(\frac{\partial C}{\partial x}\right)+v_y\left(\frac{\partial C}{\partial y}\right)=D\left(\frac{\partial^2 C}{\partial y^2}\right)\pm\frac{\partial}{\partial x}(\partial C/\partial y) \qquad [3]$$

Moreover, the dependence of the current density with concentration for mass transport conditions is;

$$j=nFD\left(\frac{\partial C}{\partial y}\right) \qquad [4]$$

And then, after taking *D* as constant along the channel length;

$$v_x\left(\frac{\partial C}{\partial x}\right)+v_y\left(\frac{\partial C}{\partial y}\right)=D\left(\frac{\partial^2 C}{\partial y^2}\right)\pm D\frac{\partial}{\partial x}\left(\frac{\partial C}{\partial y}\right) \qquad [5]$$

Since the slowest reaction is the oxygen electroreduction, we are going to study the last one as being a *rds* limited process;

$$v_x\left(\frac{\partial C}{\partial x}\right)+v_y\left(\frac{\partial C}{\partial y}\right)=D\left(\frac{\partial^2 C}{\partial y^2}\right)-D\frac{\partial}{\partial x}\left(\frac{\partial C}{\partial y}\right)+D_{H2O}\frac{\partial}{\partial x}(1-C)^2 \qquad [6]$$

When the amount of water is low, that is, at the beggining of the experiment, or the change in the oxygen concentration is not prominent, the equation reduces to:

$$v_x\left(\frac{\partial C}{\partial x}\right)+v_y\left(\frac{\partial C}{\partial y}\right)=D\left(\frac{\partial^2 C}{\partial y^2}\right)-D\frac{\partial}{\partial x}\left(\frac{\partial C}{\partial y}\right) \qquad [7]$$

Moreover and and it was stated at the beginning, we can take that the flow stream is coming along the catalyst layer, $v_y=0$ and $v_x= U^o$ (fully developed stream flow);

$$U^o\left(\frac{\partial C}{\partial x}\right)=D\left(\frac{\partial^2 C}{\partial y^2}\right)-D\frac{\partial}{\partial x}\left(\frac{\partial C}{\partial y}\right) \qquad [8]$$

$$\left(\frac{\partial C}{\partial x}\right)=\frac{D}{U^o}\left\{\left(\frac{\partial^2 C}{\partial y^2}\right)-\frac{\partial}{\partial x}\left(\frac{\partial C}{\partial y}\right)\right\} \qquad [9]$$

We can solve Eq. [10] as it or using electrochemical magnitudes. Since the concentration profile is related to the current density as follows;

$$\frac{j}{nF}=D\left(\frac{\partial C}{\partial y}\right) \text{ and } C=\frac{1}{nFD}\int j dy \qquad [10]$$

And then we obtain:

$$\frac{U^{o}}{D}\left(\frac{\partial}{\partial x}\int j dy\right)=\left(\frac{\partial j}{\partial y}\right)-\left(\frac{\partial j}{\partial x}\right) \qquad [11]$$

The solution is a parabolic cylinder profile;

$$j(x,y)=\frac{y-\frac{U^{o}y^{2}}{c_1 D}}{c_1}+\frac{x}{c_1}+c_2 \qquad [12]$$

The initial and contour conditions are required to define the constants, so we can employ the mass corrected Tafel Law to find those conditions.

$$j(x,y)=\frac{C(x,y)}{C^{o}}\,j_o\exp(-\eta(x,y)/b) \qquad [13]$$

At *y=0* and $\forall x$ the expression for *j(x,0)* is zero since we have to take that the maximum gradient is obeyed, that is, *C(x,0)*.

Then, the first initial condition is;

1.- $j(x,y=0)=0\,\forall x$ [14]

but the overpotential is different to 0, that is, the cell is working so $c_2$=0 for *x*=0;

The second contour condition arose from the necessity to achieve a maximum current for mass transport conditions at the centre of the channel, *d/2*.

2.- $j(0,y=d/2)=j_{\lim}$ [15a]

being $j_{\lim}=\frac{2nFDC^{o}}{d}$ [16]

In this case the $j_{lim}$ is variable since $C^o$ is decreasing all the time.

$\forall x$ it is valid but with lower values of $C^o$. However, for the initial *x*=0, $C^o$ can be considered as constant. Thus, it is demonstrated that:

$$c_1=\frac{d^{2}}{4nFDC^{o}}\ [\mathrm{cm^3\,A^{-1}}] \qquad [15b]$$

Finally, Eq. [12] becomes:

$$j(x,y)=\frac{4nFDC^{o}(x+y)}{d^{2}}-\frac{16U^{o}n^{2}F^{2}DC^{o2}y^{2}}{d^{4}} \qquad [17]$$

which is plotted in Figure 5a using the typical experimental figures.

Besides, from Eq. [10] we can calculate the concentration profile (Figure 5b);

$$C(x,y) = \frac{1}{nFD}\int j(x,y)dy = \frac{4C^{o}xy}{d^{2}} + \frac{2C^{o}y^{2}}{d^{2}} - \frac{8U^{o}nFC^{o2}y^{3}}{3d^{4}} + cte \qquad [18]$$

Substituting [18] and [17] into [13] we can find the overpotential (Figure 5c);

$$\eta(x,y) = b\ln\left[\frac{\frac{j_o}{d^{2}}\left(4xy + 2y^{2} - \frac{8U^{o}nFC^{o}y^{3}}{3d^{2}}\right)}{\left(\frac{4nFDC^{o}(x+y)}{d^{2}} - \frac{16U^{o}n^{2}F^{2}DC^{o2}y^{2}}{d^{4}}\right)}\right] \qquad [19]$$

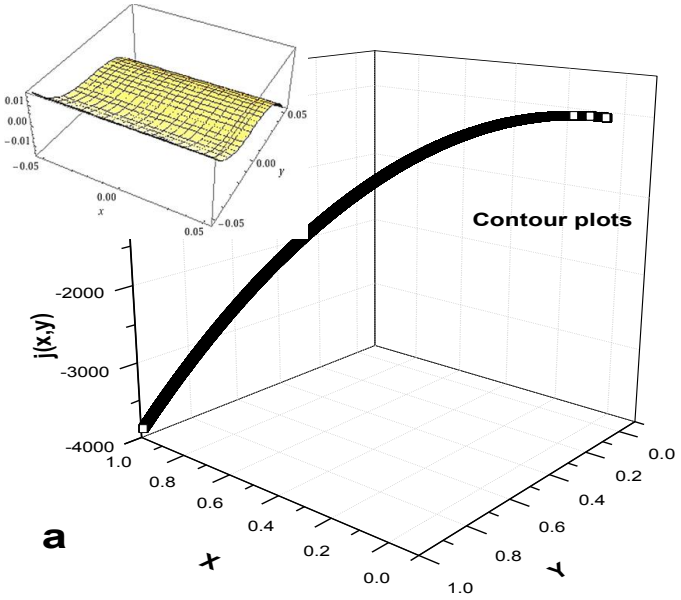


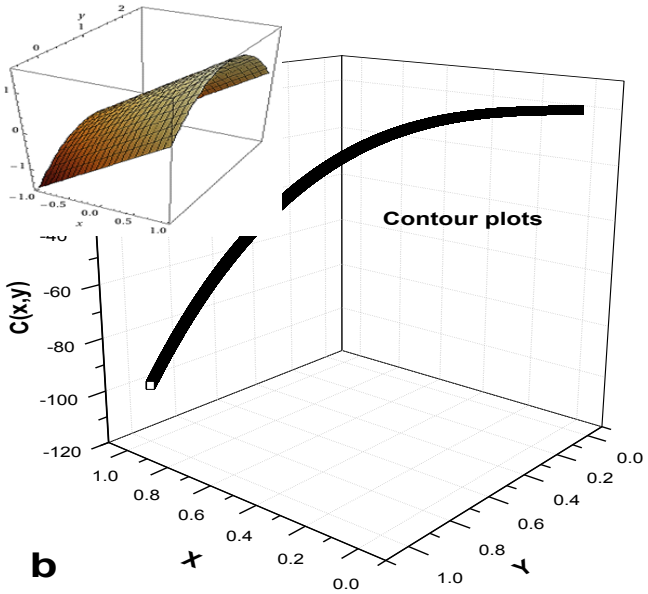

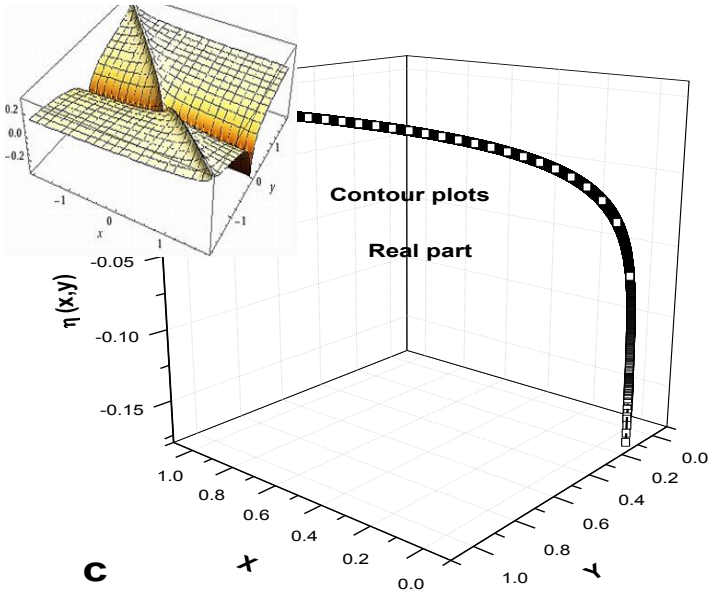


**Figure 5.-** Predicted 2 D plots for the following electrochemical properties in the cathodic catalytic layer. a.- current density *j(x,y)*, b.- Concentration, *C(x,y)* and c.- overpotential *η(x,y)* profiles. Inset images show 3 D evolving lines and Real part contour plots.

The used experimental values are those deduced from the analysis of the gas flow system and electrode reactions; $U^o$= 0.16 cm $s^{-1}$, $D$=0.02 $cm^2$ $s^{-1}$ , $C^o$= $10^{-3}$ mol $cm^{-3}$ [24, 25]. For the home made PEM fuel cell the mean value of was $d$=0.20 cm, however distinct values have been changed to check for the theoretical prediction [26]. This has been also applied for $L$.

Large values of oxygen diffusivity, $D$, in the diffusion layer were found, that is, 0.02 $cm^2s^{-1}$ and in the case of lower $U^o$ values, expected D figures were found: 0.001 $cm^2s^{-1}$. The obtained diffusivity is rather lower than that reported before [27, 28], however if we take into account the Bruggeman´s correction of porosity ($D_{eff} = \varepsilon^{3/2}D$) being ε the mean porosity factor of the membrane electrode assembly, ca. 1/3, is approximately the half of ours (0.26 $cm^2s^{-1}$). Thus, it is likely that the difference arose from the distinct roughness and porosity of our columnar platinum surfaces. Besides, using the proton and oxygen transport analysis based on the Cairns-Perry-Newman [18] in a 1 D fuel cell model, Kulikovsky [29] found a porosity factor of only 6.3 % with a similar value (0.27 $cm^2s^{-1}$) of the binary diffusivity (oxygen-nitrogen in air) at 60°C taking pore saturation conditions. In this case there is also no formation of columnar platinum structures, at least as they did not reported them there.

Besides, we also need experimental magnitudes of $j_o$ since $C^o$ is retained as constant an arbitrarily 1 M as the maximum initial proton activity. The determination of the first magnitude is common in Electrochemistry and in the case of fuel cell is well described elsewhere [30, 31] and also for gas diffusivities detailed above [32, 33]. Thus, the measurement of cathodic $j_o$ at the beggining of the experiment and after 1 month was 0.5 A $cm^{-2}$ and 0.7 A $cm^{-2}$, respectively. The larger value after 1 month was not totally expected for high catalyst roughness, but thinking on the possibility of oxygen adsorption parallel to the surface, the presence of large columns with not small voids yields a higher extent of adsorption and ulterior reaction.

Nevertheless, the perpendicular oxygen adsorption is not expected since in the space between columns further lateral interactions probably shield the process.

One of the most important and characteristic parameters in an electrochemical reactor is the Wagner number, **Wa**, since it rationalizes 2 types of resistances. The uniformity of this number gives a well-defined secondary current distribution [34, 35]. The polarization resistance $R_p$ is the ratio between the Tafel slope $b$ (containing the charge transfer coefficient $\alpha$, that is, $b=RT/\alpha F$) and $j_o$. The other is related to the ohmic resistance $R_\Omega$, classically determined.

$$Wa = \frac{b / j_o}{R_\Omega} \qquad [20]$$

In this paper, $R_\Omega$ was measured by impedance spectroscopy [21] at the beginning and after 1 month of continuous operation, being 0.04 and 0.12 $\Omega$ cm$^2$. The constant Tafel slope of 0.03 V dec$^{-1}$ was similar at the beginning and after 1 month of operation. It was determined using the steady state potentiostatic method after reaching constant current values from each potential step starting at the open circuit downwards [34, 35]. It is important to notice that $j_o$ diminishes but the Tafel slope remains the same, showing that the mechanism of the process is unaltered, but not the kinetics. In this sense, the change in the morphology and surface area of the platinum electrode at both stages of the fuel cell operation can be also responsible of this change in $j_o$. The evaluation of the surface area by the carbon monoxide *stripping* methodology does not give additional mistakes in spite of a change in the morphology from smooth to columnar profiles. Thus, **Wa** changes from 1.5 (typical of a rather uniform secondary current distribution) as shown in Figure 5a to 0.36 showing a no uniformity, so a different approach is needed as we are going to encourage below (Section 3.3) for a columnar electrode instead of a smooth and flat surface.

The operation curve is presented here below as Figure 5d. The only difference with respect to the experimental values arose from those near the open circuit potential. For larger currents the predicted potentials are slightly higher, that is, ca. 2-5 % larger than those experimentally found. Thus, it will be necessary to introduce distinct velocity profiles to that of $U^o$ as it is going to be done in another paper.

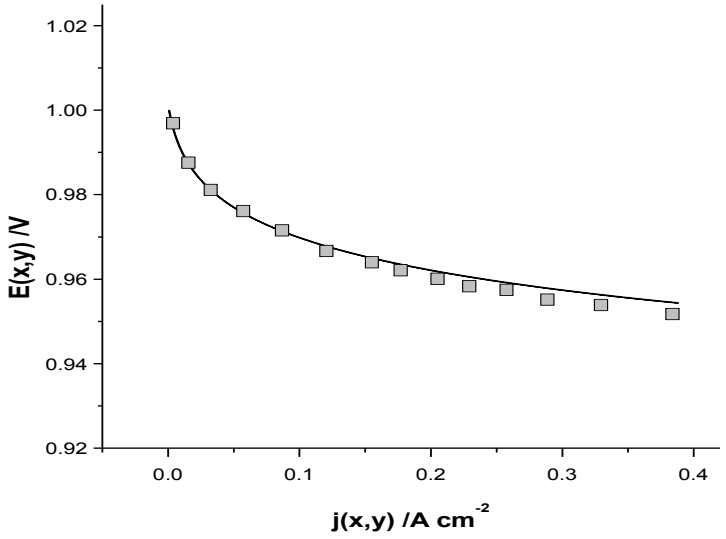


**Figure 5d.-** PEM fuel cell performance (operation curve) as electric potential, *E(x,y) vs*. current density, *j(x,y)* using the equations find for a fully developed stream condition on smooth electrodes. Experimental points determined as explained in the Experimental Section.

### 3.2.- Current, concentration and overpotential profiles along the 2D channel under full operation.

The mass balance equation is now;

$$v_x\left(\frac{\partial C}{\partial x}\right)+v_y\left(\frac{\partial C}{\partial y}\right)=D\left(\frac{\partial^2 C}{\partial y^2}\right)-D\,\frac{\partial}{\partial x}\left(\frac{\partial C}{\partial y}\right)+D_{H2O}\,\frac{\partial}{\partial x}(1-C)^2 \qquad [21]$$

When the flow stream is coming along the catalyst layer, $v_y=0$ and $v_x= U^o$:

$$\left[1+2\,\frac{D_{H2O}}{U^o}(1-C)^2\right]\left(\frac{\partial C}{\partial x}\right)=\frac{D}{U^o}\left\{\left(\frac{\partial^2 C}{\partial y^2}\right)-\frac{\partial}{\partial x}\left(\frac{\partial C}{\partial y}\right)\right\} \qquad [22]$$

This equation has been solved likewise that above obtaining a similar solution;

$$j(x,y)=\frac{4nFDC^{\,o}(x+y)}{d^2}-\frac{16\,(U^o+2D_{H2O})n^2F^2DC^{o2}y^2}{d^4} \qquad [23]$$

In this case it is convenient to use the Stefan-Maxwell interdiffusion coefficients, that is, *D* is the single value but $D_{H2O}$ is that of water in oxygen [19, 24]. This value and those of oxygen at the membrane interphase are different from those measured in a pure phase, that is 3 orders lower due to the working temperature and type of membrane [25].

The shapes and profiles of current density, concentration and overpotential as a function of *x* and *y* are nearly the same.

$$C(x,y) = \frac{1}{nFD}\int j(x,y)dy = \frac{4C^{o}xy}{d^{2}} + \frac{2C^{o}y^{2}}{d^{2}} - \frac{8(U^{o} + 2D_{H2O})nFC^{o2}y^{3}}{3d^{4}} + cte \qquad [24]$$

$$\eta(x,y) = b\ln\left[\frac{\frac{j_o}{d^{2}}\left(4xy + 2y^{2} - \frac{8(U^{o} + 2D_{H2O})nFC^{o}y^{3}}{3d^{2}}\right)}{\left(\frac{4nFDC^{o}(x+y)}{d^{2}} - \frac{16(U^{o} + 2D_{H2O})n^{2}F^{2}DC^{o2}y^{2}}{d^{4}}\right)}\right] \qquad [25]$$

Evidently the electrochemical and mass profiles are similar to those denoted above.

**3.3. Columnar platinum catalyst microprofile.**

We are going to convert the 2 D mass transport differential equations above to a single variable dependent formula using the curvilinear parametrization of a trochoid:

$$x(t) = \alpha(t - \lambda\sin t) \quad \text{and} \quad y(t) = \alpha(1 - \lambda\cos t) \qquad [26a,b]$$

Being $\alpha$ the radius of the trochoid and $\lambda$ the "path" of the curvilinear line. Since the circle of radius $\alpha$ rolls without slipping along a hypothetical line (catalyst support base in our case), the centre of the circle moves parallel to this line. Every point of this rotating plane attached to the circle defines the parametric curvilinear line (trochoid or cycloid). In our case, the path is ½. We are going to envisage all the treatment with this value. If the path is larger, the current density or concentration profiles reach larger values, that is, for $\lambda<\alpha$ it defines a *curtate* or contracted trochoid. The opposite situation is observed for $\lambda>\alpha$ described as a *prolate* of enlarged trochoid, where the current or concentration values are lower than in the case of the geometric description of a common trochoid (or cycloid).

Then, the first derivation is;

$$x'(t) = \alpha(1 - \lambda\cos t) \quad \text{and} \quad y'(t) = \alpha\lambda\sin t \qquad [27a,b]$$

With the following partial derivatives:

$$\left(\frac{\partial C}{\partial x}\right) = \left(\frac{\partial C}{\partial t}\right)\frac{1}{\alpha(1 - \lambda\cos t)};\ \left(\frac{\partial C}{\partial y}\right) = \left(\frac{\partial C}{\partial t}\right)\frac{1}{\alpha\lambda\sin t} \text{ and } \left(\frac{\partial^{2}C}{\partial y^{2}}\right) = \left(\frac{\partial^{2}C}{\partial t^{2}}\right)\frac{1}{\alpha\lambda\cos t}$$

[28a,b,c]

**3.3.1.- Concentration, current and overpotential profiles for fully developed stream along the surface at the early stages of electrode reactions.**

In the case of the PEM fuel cell fully working at early stages, the originated current density can be expressed as a change in the oxygen concentration as said before;

$$v_x\left(\frac{\partial C}{\partial x}\right)+v_y\left(\frac{\partial C}{\partial y}\right)=D\left(\frac{\partial^2 C}{\partial y^2}\right)\pm D\,\frac{\partial}{\partial x}\left(\frac{\partial C}{\partial y}\right) \qquad [7]$$

with the partial derivatives expressed in Eqs. [28a,b,c] and the following cross-derivation;

$$\frac{\partial}{\partial x}\left(\frac{\partial C}{\partial y}\right)=\left(\frac{\partial^2 C}{\partial t^2}\right)\frac{1}{\alpha^2(\lambda\sin t-\lambda^2\cos t\sin t)} \qquad [28d]$$

Using the condition of $v_x=U^o$ and $v_y=0$;

$$\left(\frac{\partial C}{\partial t}\right)\frac{U^o}{\alpha(1-\lambda\cos t)}=D\left(\frac{\partial^2 C}{\partial t^2}\right)\left[\frac{1}{\alpha\lambda\cos t}-\frac{1}{\alpha^2(\lambda\sin t-\lambda^2\cos t\sin t)}\right] \qquad [29]$$

As this equation has no rigorous solution and to study current density profiles we will apply the Clairaut´s Theorem of substitutions using the auxiliary derivative function; *j(t)=C´(t)* as an alternative function. This theorem allows to obtain one of the likely resolutions after further integration, since this auxiliary function is the tangent of the solutions´ family of curves.

$$\frac{U^o}{\alpha(1-\lambda\cos t)}\,j(t)=D\left[\frac{1}{\alpha\lambda\cos t}-\frac{1}{\alpha^2(\lambda\sin t-\lambda^2\cos t\sin t)}\right]\left(\frac{\partial j(t)}{\partial t}\right) \qquad [30]$$

We can factorise this expression to:

$$j(t)=\frac{D}{U^o}\left[\frac{(1-\lambda\cos t)}{\lambda\cos t}-\frac{(1-\lambda\cos t)}{\alpha(\lambda\sin t-\lambda^2\cos t\sin t)}\right]\left(\frac{\partial j(t)}{\partial t}\right) \qquad [31]$$

And solved it using the initial condition, *j(0)=1*;

$$j(t)=\exp\left(\frac{\lambda(\log(\alpha(\lambda-1)t+1)-\alpha(\lambda-1)t)}{\alpha(\lambda-1)^2\frac{D}{U^o}}\right) \qquad [32]$$

We can plot the function for the usual values of *D* and $U^o$ shown above and the experimental values for the trochoid (Figure 6);

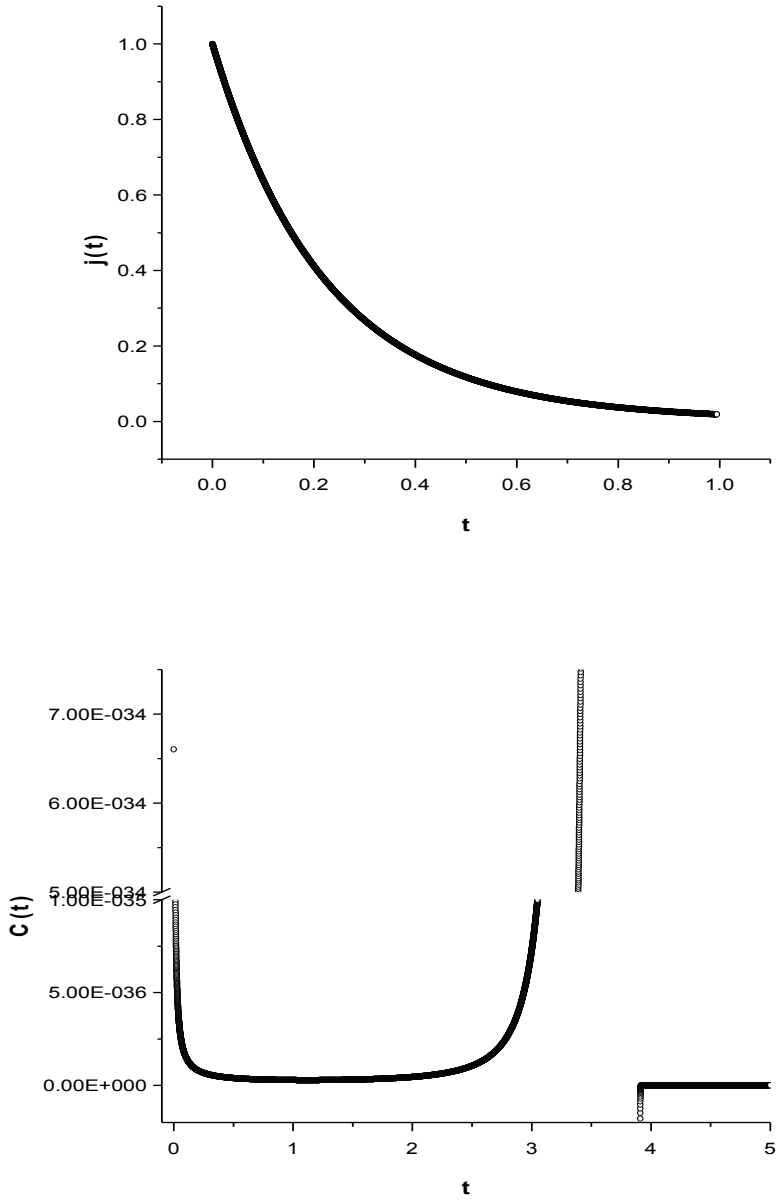


**Figure 6.-** a.- Current density, *j(t)* and b.- concentration, *C(t)* for a single parametric variable dependence.

The integrated expression renders the initial concentration profile;

$$C(t) = \frac{1}{nFD}\int \exp\left(\frac{\lambda(\log(\ \alpha(\lambda-1)t+1)-\alpha(\lambda-1)t)}{\alpha(\lambda-1)^2\dfrac{D}{U^o}}\right)dt \qquad [33]$$

$$C(t) = -\frac{1}{nFD}\frac{\alpha(\lambda-1)^2\frac{D}{U^o}}{\alpha\lambda(\lambda-1)}\left(e\alpha(\lambda-1)t+e\right)^{\frac{\lambda}{\alpha(\lambda-1)^2\frac{D}{U^o}}}\left[\frac{\lambda(\alpha(\lambda-1)t+1)}{\alpha(\lambda-1)^2\frac{D}{U^o}}\right]^{-\frac{\lambda}{\alpha(\lambda-1)^2\frac{D}{U^o}}} *$$

$$\Gamma\left(\frac{\lambda}{\alpha(\lambda-1)^2\frac{D}{U^o}}+1,\frac{\lambda(\alpha(\lambda-1)t+1)}{\alpha(\lambda-1)^2\frac{D}{U^o}}\right)$$

[34]

And simplifying for $\alpha = \lambda = 0.5$

$$C(t) = \frac{1}{nFD}\left\{t + \frac{4\exp\left[\frac{4}{\frac{D}{U^o}}\right]\Gamma\left(4+\frac{\frac{D}{U^o}}{\frac{D}{U^o}},\frac{4}{\frac{D}{U^o}}\right)}{\left[\frac{4}{\frac{D}{U^o}}\right]^{\frac{0.5+0125\frac{D}{U^o}}{0.125\frac{D}{U^o}}}}\right\}$$

[35]

The plotting of the concentration profile for the usual values of $D$ and $U^o$ is near a straight line. This approach was rather simple then we also need an approximation at $t$=infinite, and then the found solution after neglecting the higher terms is;

$$C(t) = \frac{t^{\frac{\lambda+\alpha(\lambda-1)^2\frac{D}{U^o}}{\alpha(\lambda-1)^2\frac{D}{U^o}-1}}e^{\frac{-\alpha(\lambda-1)\lambda t}{\alpha(\lambda-1)^2\frac{D}{U^o}-\frac{\lambda}{\alpha(\lambda-1)^2\frac{D}{U^o}-1}}}\left(e\alpha(\lambda-1)t+e\right)^{\frac{\lambda}{\alpha(\lambda-1)^2\frac{D}{U^o}}}}{\left(\frac{\alpha(\lambda-1)\lambda t+\lambda}{\alpha(\lambda-1)^2\frac{D}{U^o}}\right)^{\frac{\lambda}{\alpha(\lambda-1)^2\frac{D}{U^o}}}}\left\{-\frac{\left[\frac{(\lambda-1)\lambda}{(\lambda-1)^2\frac{D}{U^o}}\right]^{\left(\frac{\alpha(\lambda-1)^2\frac{D}{U^o}+\lambda}{\alpha(\lambda-1)^2\frac{D}{U^o}-1}\right)}(\lambda-1)\frac{D}{U^o}}{\lambda}\right\}$$

[36]

The function is very complex to analyze since it has a strong imaginary part, however it is clear that the function has a singularity point near $t$=4 with a discontinuity starting at 3.45. The real part for large values of $t$ is practically zero (most of the reaction takes place at the edge or valley of the platinum column), but there is a large increase in the concentration after this certain point indicating an overestimation of concentrations near the edge of the validity of the equation that has not to be considered here since it has no physical meaning.

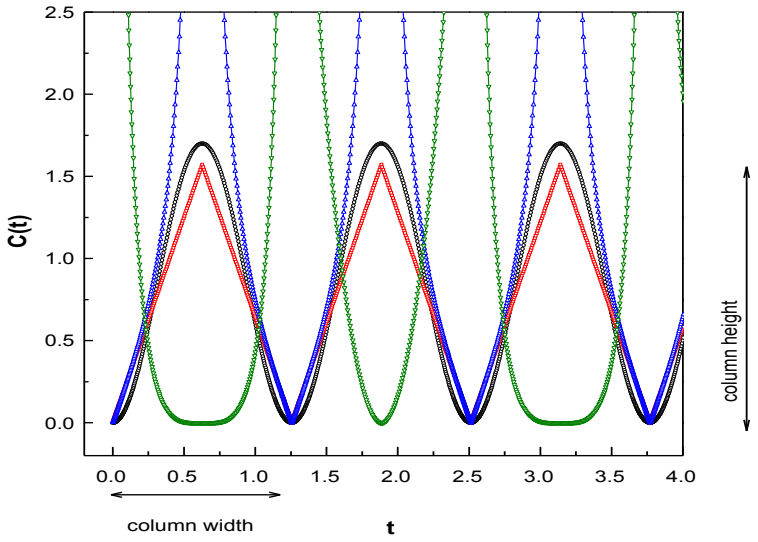


**Figure 7.-** Concentration parametric profile, *C(t)* on a trochoidal columnar surface. The curvilinear surface was defined using experimental $\lambda$=0.5 and $\alpha$=0.5. The concentration solutions are plotted for the complete surface profile along *t* with different physicochemical parameters. $D>>U^o$ (black lines); $D<<U^o$ (blue lines); $D<U^o$ (red lines) and $D...U^o$ (green lines).

Figure 7 (green lines) shows a special case of ($\alpha = \lambda = 1/2$) for *D* aprox. $U^o$. This condition is difficult to be likely since the active species has to reach the top of the trochoid to accomplish the predicted negligible *C(t)*. Anyway, when the cell is working at an initial starting condition not reaching stationary regimes, the lowest *C(t)* value has to be everywhere, therefore, it seems that at the bottom of the surface the reactant is confined and can react easily and fastly.

In the situation of $D<<U^o$ (blue lines) we are able to observe singularity points near the top of the columnar surface. Thus, at the top of the trochoid it is observed a maximum *C(t)* of the active species not well converted since the flow velocity is very fast. Thus, the value of the limiting velocity is much higher than that of what the concentration can change or react at the platinum columnar surface. This value of $U^o$ that produces the uncertainty is different depending on the shape of the trochoid, *i.e.* it depends on the values of $\alpha$ and $\lambda$. However, this singularity disappears for values of $U^o$ not much larger than *D* (red lines) mimicking the macroprofile shape of the columnar structure. Similar profiles are observed for $D>>U^o$ (black lines) denoting that surface diffusion is an important factor for the electrode conversion process.

This situation is expectable since the ratio between both parameters is related to the Reynolds number, **Re**, for the confined gas stream. Depending on this relationship we also have various Graetz numbers, **Gz**, since it relates the width, *d*, and length, *L*, of the channel. Thus,

$$Gz = \frac{d}{L}\mathrm{Re}\ Sc = \frac{d}{L}Pe \qquad [37]$$

The uniformity and moderately medium values of **Gz** or **Re** yields a homogeneous distribution of flowing stream and we can considered it as a laminar flow condition even when the parabolic profile is not completely attended. The ratio **h**=*d/L* is called the dimensionless characteristic length of the fat 2 D fuel cell. In our case *d*=0.20 cm and *L*=25.15 cm, so is 0.00795.

Besides, for **Re** we know that it strongly depends on the value of the flow velocity, and for instance $U^o$= 0.16 cm $s^{-1}$ and $\nu$=0.01 $cm^2$ $s^{-1}$, the **Re**= 402.4. This value of **Re** is rather low for common hydraulic systems but not in fuel cell devices [36-38]. Thus, those values lower than 600 are enough to complete the access of oxygen throughout the channel length. In the case of this fuel cell manufacturised at the lab it was possible to increase the value of $U^o$ 1 order more.

Moreover, **Sc** = 0.01 $cm^2 s^{-1}$/0.02 $cm^2$ $s^{-1}$ = 0.5. For **Gz** the definition shows that with **h**= 0.00795, **Re**= 402.4 and **Sc** = 0.5, then **Gz** = 1.6. This value is rather low for usual pipelines studies but not for 2 D fuel cells.

On the same direction the study of the *j(t)* profile with distinct values of *D* and $U^o$ renders a similar analysis (Figure 8). When the limiting velocity is large the diffusivity gets flush and the current profile shows very little values that suddenly increase near the top of the platinum column (green lines, $D/U^o=10^{-2}$). On the other hand, for the opposite case there is a smooth increase in the current value since the hydrodynamic conditions dominate the experimental conditions, black and red lines ($D/U^o=10^4$ and $10^2$), that almost coincides independent on the limiting velocity value. This means that there is a saturation of the current after a certain hydrodynamic rate. When both diffusivity and hydrodynamic conditions are equivalent it resembles the profile of the columnar surface geometry (blue lines), showing a combination of both behaviours.

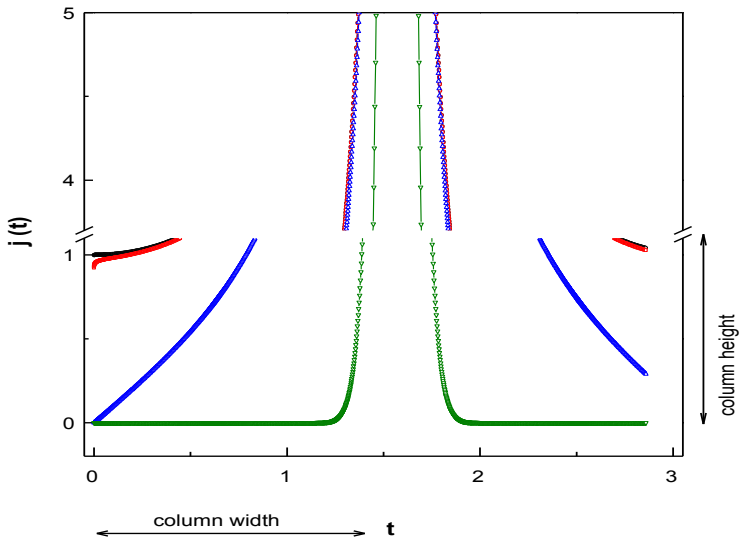


**Figure 8.-** Current density *j(t)* parametric profile on a trochoidal columnar surface defined by λ=0.5 and α=0.5. The current shapes were found with different physicochemical parameters. $D/U^o=10^4$ (black lines); $D/U^o=10^2$ (red lines); $D/U^o=1$ (blue lines) and $D/U^o=10^{-2}$ (green lines).

Due to the complexity of the concentration profile we are going to deduce the overpotential shape only for our case of $\alpha = \lambda = 0.5$ using Eq. [13] and applying Eqs. [32] and Eqs. [36, 37];

$$\eta(t) = b \ln \left( \frac{\left( \frac{t}{nFD} + \frac{4}{nFD} \left[ \frac{4}{\frac{D}{U^o}} \right]^{-\frac{0.5+0125\,\frac{D}{U^o}}{0.125\,\frac{D}{U^o}}} \exp\left[ \frac{4}{\frac{D}{U^o}} \right] \Gamma\left( \frac{0.5 + 0.125\,\frac{D}{U^o}}{0.125\,\frac{D}{U^o}}, \frac{4}{\frac{D}{U^o}} \right) \right)}{\exp\left( \frac{4(\log(1 - 0.25\,t) + 0.25\,t)}{\frac{D}{U^o}} \right)} \right) + b \ln\left( \frac{j_o}{C^o} \right)$$

[38]

Using $b$= 0.03 V dec$^{-1}$, $j_o$=0.5 A cm$^{-2}$; $C^o$= 10$^{-3}$ mol cm$^{-3}$, we can estimate Eq. [38] to simpler formulae to make the plotting easier (not shown here). Figure 9 a and b plot the overpotential contours with those expressions for small and large $t$ values, but the exact equation [38] covers the values of both graphs.

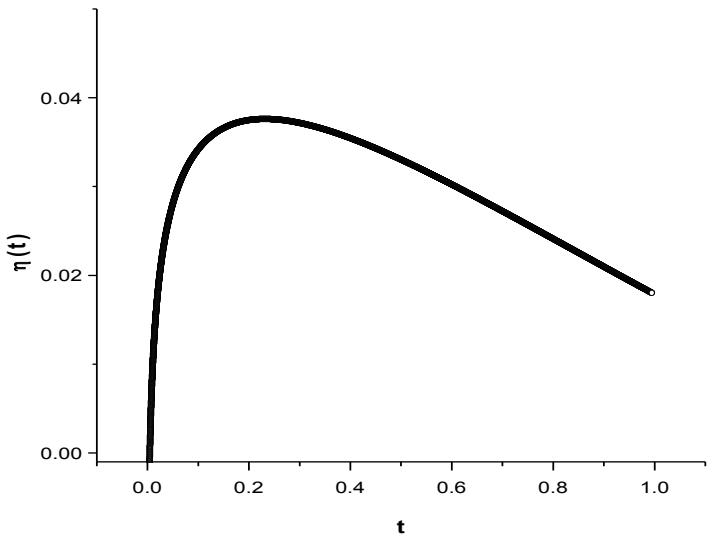

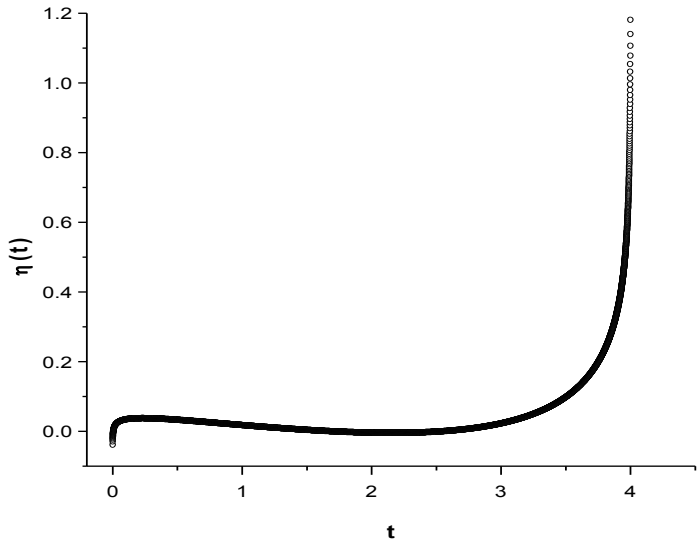


**Figure 9.-** a and b.- overpotential profile $\eta(t)$ at small and large values of the parametric variable *t*.

At the beginning of the parametric variable there is a non-uniformity of the potential distribution, whereas between *t*=1 and the singular point at *t*=3.45 the shape is rather homogeneous. For *t* greater than 3.5 there is a sudden increase in the overpotential contour, and for values higher than 4 the singularity makes the solution diverging.

Figure 10a exhibits the polarization curve of the fuel cell after 1 month of continuous operation. The overpotentials were selected for small *t* figures and the current densities calculated accordingly. The experimental points were obtained as explained in the Experimental Section. It is clear that the only part that is well mimicked is the starting of the curve near the open circuit value, that is, low current densities. Besides, the ohmic drop region is fairly well described near those values, however the growth in current densities makes wider the gap between theoretical and experimental figures.

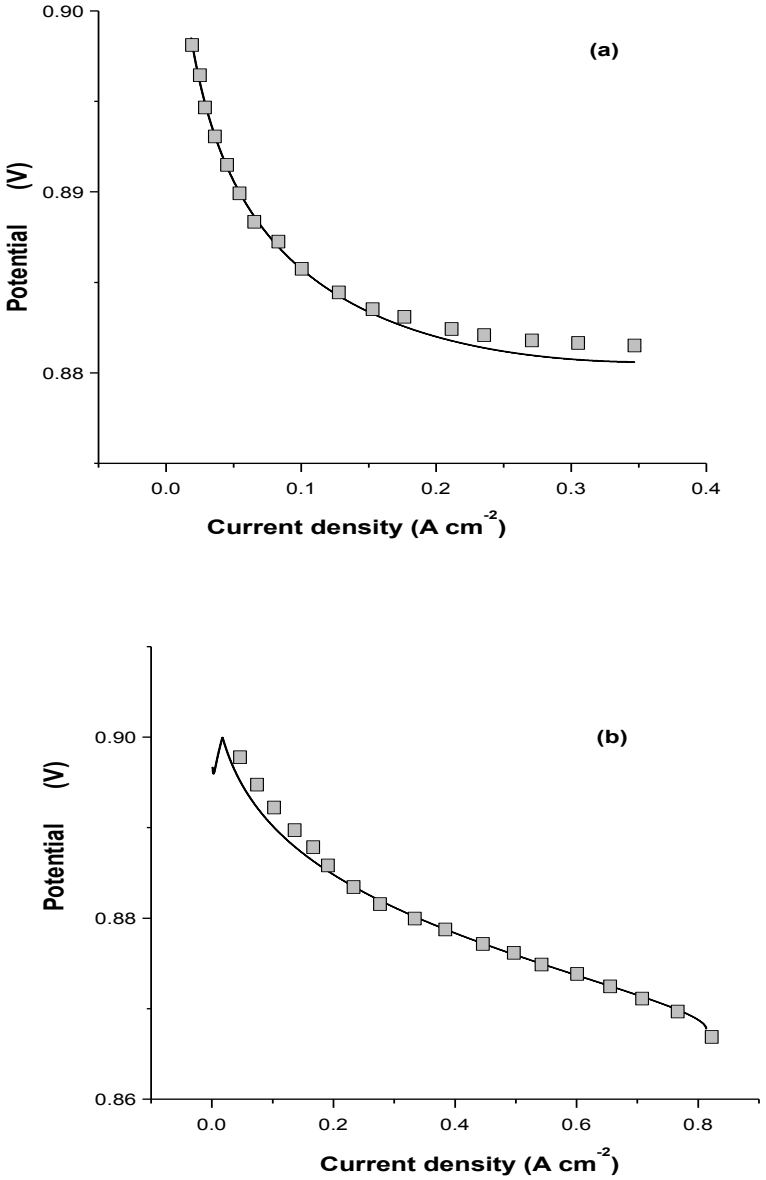


**Figure 10.-** a and b.- polarization curves of the fuel cell using the overpotential approaches for small and large *t* values, respectively, and current density profiles shown in Figure 8.

However, we can apply analytical equations or the approximation for large *t* values, it is possible to reproduce mostly the regions of the ohmic drop zone as shown in Figure 10b. This zone renders a good concordance with the specific resistance found experimentally. Though, using this equation some experimental data near the open circuit potential are overestimated so in this region is better to employ the other approach of small *t* values.

In spite of the almost complete prediction of the polarization curve, the problem of attaining a limiting current density is not appearing completely after linking Eqs. [38] and [32]. In this sense, analytical expressions distinct to $U^o$, *i.e.* tangential and normal velocities dependent on 2 variables or a single parametric one are encouraged in another paper to better modelling the 2 D PEM fuel cell operation.

**4. Conclusions.**

Mass transfer equations at the beginning and after long time periods were solved for smooth catalytic surfaces introducing the Clairaut Theorem and applying the contour condition of zero current density at the origin and maximum at the half of channel width. For both conditions a parabolic cylinder profile was obtained, only adding the water interdiffusion coefficient for long time operations but not the electroosmotic drag coefficient. The employ of a fully developed velocity condition overestimates the ohmic drop region for these smooth electrodes, so a 2 D coordinate dependent velocity components are going to be further advanced.

Current, concentration and overpotential profiles for the PEM fuel cell operation after 1 month on cathodic catalytic layers have been theoretically envisaged under steady state regimes. For this purpose the variable change in the mass balance differential equations was achieved using the parametric curvilinear description of a trochoid imitating the columnar electrodes. The analytical solutions were compared with experimental values obtained using a home-made hydrogen/oxygen polymeric membrane cell. Two regions for the solution of the concentration profile were obtained with a discontinuity behaviour at a certain value, up from and lower than that, two potential behaviours were separated from which two polarization curves for the fuel cell were plotted. The one at lower figures well describes current and potentials near the open circuit point, whereas the solution for larger parameterized values better represents the ohmic drop zone with values of cell resistances similar to the experimental ones.

**5.- Experimental Section.**

A single PEM fuel cell was used of 200 $cm^2$ geometric areas, with a MEA 10 cm x 20 cm effective geometric area and 183 microns thickness. The geometric characteristics of the bipolar plates in the home made cell were measured and calculated in the laboratory, but some experiences were conducted with distinct widths and depths for comparisons. The channel length was 25.15 cm, the channel depth 0.15 cm and the width of 0.20 cm. Besides, the indirect determination of catalyst and gas diffusion layers yields 12 and 230 microns, respectively.

The catalyst had 0.4 to 2.1 mg $cm^{-2}$ platinum loads on anode and 0.4 to 3.6 mg $cm^{-2}$ on cathode catalyst layers. The high loads of platinum allow the formation of columnar platinum structured surfaces. The preparation of the MEA was achieved as detailed elsewhere [27] with Nafion 117 or 212 from Du Pont using our cleaning method. Thus, the membranes were firstly boiled for 30 min in acidic 3 % hydrogen peroxide and later for the same period with concentrated $HNO_3$. To eliminate the residues, the ensembles were repeatedly boiled in MilliQ water for 1 hr. at 80$^oC$, followed by immersion in 0.10 M HCl (analytical grade from Merck) for 24 hrs. and recurrently rinsed in double Millipore $MilliQ^+$ water at ambient temperature.

A classic control of the real exposed area was conducted using the oxidative desorption of carbon monoxide (99.997 %, < 2ppm $C_xH_y$ from Linde Group). Adsorption experiments were conducted after gas bubbling over and in a 0.50 M sulphuric acid as supporting electrolyte until saturation (5 min) without the presence of either the auxiliary (large platinum foil) or reference (capillary hydrogen platinum ensemble) electrodes to evade

impurities. The oxidative voltammetric contour at a 0.010 $Vs^{-1}$ scan rate from the residues (anodic *stripping* experiments) was plotted at an adsorption potential of 0.05 V held for 2 min. The excess of dissolved carbon monoxide was removed with continuous argon bubbling (N50 from Air Liquide) and instantaneously switching the solution with the supporting electrolyte keeping all the time the potential at 0.05 V. The active surface area of anodic and cathodic sides of the MEA were determined from the ratio of the charge involved in the carbon monoxide anodic stripping voltammetric shape from 0.60 to 1.50 V (taking saturation for 2 e equal to 420 $\mu C\ cm^{-2}$) after the subtraction of the double layer charging contribution [22].

The 200 $cm^2$ PEM fuel cell in the long-term investigations was a home-made device constructed using a compact MEA preparation (Nafion 117 or 212, pressed with different platinum loads on the cathodic and anodic sides) spending a temperature-controlled hydraulic press. The working temperature was varied from 60 to 85$^oC$. The humidified oxygen and hydrogen streams (up to 99.99 % purity of Linde Group) were thermostatted before the entrance of the fuel cell operating at ca. 68$^oC$ and occasionally at 80$^oC$. The polarization curves of PEM fuel cell were obtained using a PGZ Potentiostat-galvanostat-impedance analyser from Radiometer Copenhagen (Program Voltalab 32 System), occasionally with the coupling of a current and voltage booster for large values. The curves were recorded using the galvanodynamic method, that is, imposing increasing current steps, from 0.1 to 1.0 μA (depending on the curve section) for at least 2-3 min to range constant cell potentials between the open circuit values (ca. 0.98 V for full hydration) and the lowest possible, *i.e.* 0.15 V. The same equipment was used to obtain cyclic voltammetries of the anodic and cathodic electrodes in oxygen free 0.50 M sulphuric acid at the begging of the experiments and after 1 month of continue operating at near 0.96 V (low currents). The control of the cleanness and purity of the system was performed by a repetitive cyclic voltammetry. The curves were run from 0.05 V to 1.50 V at 0.10 V $s^{-1}$ starting the scan at the open circuit value downwards in the cathodic direction and then upwards from 0.05 V. As expressed above distinct platinum loads were assayed from 0.4 to 3.6 mg $cm^{-2}$, but only the results for the latter are shown here, since they are the ones that exhibit columnar morphologies after certain periods of work. The experiments shown here respond to the cathodic platinum electrode since the mass balances are analysed for this reaction.

**Declaration of Competing Interest** The author declares that he has no known competing financial interests or personal relationships that could have appeared to influence the work reported in this paper.

**Acknowledgements** This research was supported by PEDECIBA (Programa de Desarrollo de Ciencias Básicas) from Uruguay- United Nations.

**Keywords**; columnar electrodes, fuel cells, trochoids, current distribution, differential equations.

**References.-**

[1] W. Ng, M. Patil, A. Datta, *J. Amer. Helicopter Soc.* **2021,** *66*, 012009.

[2] O. Shakouri, M. Hossein Ahmadi, M. Farzaneh Gord, *Int. J. Low-Carbon Technol.* **2021,** *16,* 417–428.

[3] S. Matsuda, Y. Niitsuma, Y. Yoshida, M. Umeda, *Sci. Rep*. **2021,** *11,* 8382-8390.
[4] Springer Handbook of Electrochemical Energy, Cornelia Breitkopf, Karen Swider-Lyons (Eds.) Berlin: Springer Ed., **2017,** ISBN 978-3-662-46657-5.
[5] P. Trogadas, J. I. S. Cho, N. Kapil , L. Rasha, A. Corredera, D. J. L. Brett, M. –O. Coppens, *Sustain. Energy Fuels*, **2020,** *4,* 5739-5746.
[6] M. E. Martins, R. C. Salvarezza, A. J. Arvia, *Electrochim. Acta*, **1997,** *43,* 549-561.
[7] M. E. Martins, C. F. Zinola, G. Andreasen, R. C. Salvarezza, A. J. Arvia, *J. Electroanal. Chem*. **1998,** *445,* 135-154.
[8] A. Kulikovsky, *Electrochim. Acta* **2004,** *49,* 617-625.
[9] T. Reshetenko, A. Kulikovsky, *Electrochem. Commun*. **2019,** *101,* 35-38.
[10] A. Kulikovsky, *Electrochim. Acta* **2014**, *130,* 826-829.
[11] Andrei Kulikovsky, *J. Electroanal. Chem*. **2014,** *720-721,* 47-51.
[12] G. Maranzana, J. Mainka, O. Lottin, J. Dillet, A. Lamibrac, A. Thomas, S. Didierjean, *Electrochim. Acta* **2012,** *83,* 13-27.
[13] J. Mainka, G. Maranzana, J. Dillet, S. Didierjean, O. Lottin, *J. Power Sources,* **2014,** *253,* 381-391.
[14] S. Chevalier, C. Josset, A. Bazylak, B. Auvity, *J. Electrochem. Soc.* **2016,** *163,* F816-F823.
[15] E.L. Gyenge, *J. Power Sources* **2005,** *152,* 105–121.
[16] S. Chevalier, C. Josset, B. Auvity, *Renew. Ener.* **2018,** *125,* 738-746.
[17] J. Xuan, H. Wang, D.Y.C. Leung, M.K.H. Leung, H. Xu, L. Zhang, Y. Shen, *J. Power Sources* **2013,** *231,* 1-5.
[18] M. L. Perry, J. Newman, E. J. Cairns, *J. Electrochem. Soc.,* **1998**, *145,* 5-15.
[19] R. B. Bird, W. E. Stewart, E. N. Lightfoot, Transport Phenomena, **1960**, p. 542, John Wiley & Sons, Inc., New York.
[20] K.T. Jeng, S.F. Lee, G.F. Tsai, C.H. Wang, *J. Power Sources,* **2004,** *138,* 41–50.
[21] S. Chevalier, C. Josset, A. Bazylak, B. Auvity, *J. Electrochem. Soc.*, **2016**, *163***,** F816-F823.
[22] C. F. Zinola, *J. Electrochem. Soc*. **2017**, *164,* H170-H182.
[23] C. F. Zinola, *ChemPhysChem*, **2011,** *12,* 172 – 183.
[24] H. Ju, C-Y. Wang, *J. Electrochem. Soc.*, **2004**, *151***,** A1954-A1960.
[25] R. Harris, L. A. Woolf, *J. Chem. Soc. Faraday Trans. 1 Phys. Chem. Condens. Phases*, **1980,** *76*, 1348-1353.
[26] C. F. Zinola, On the description of a 2-D thin layer velocity, concentration and current profile under an isothermal laminar flow, *Int. J. Heat Mass Transf*., submitted.
[27] E. Teliz, V. Diaz, I. Pérez, M. Corengia, C. F. Zinola, *Int. J. Hydrogen Ener*. **2012,** *37,* 14761-14768.
[28] K.T. Jeng, S.F. Lee, G.F. Tsai, C.H. Wang, *J. Power Sources*, **2004,** *138*, 41–50.
[29] A. A. Kulikovsky, *Electrochem. Solid-State Lett*. **2009,** *12*, B53-B56.
[30] F. Barbir, in PEM Fuel Cells; Theory and Practice (Second Edition), **2013,** Chapter Three - Fuel Cell Electrochemistry, Pages 33-72. Elsevier Science, ISBN 978-0-12-387710-9, Academic Press.
[31] A. A.Kulikovsky, Analytical Modelling of Fuel Cells (Second edition), **2019**, Pages 1-33 Chapter 1 - Fuel cell basics, Elsevier Science, ISBN 978-0-444-642226, Elsevier Print.
[32] E. N. Fuller, P. D. Schettle, J. C. Giddings, *Ind. Eng. Chem.* **1966,** *58,* 19–27.
[33] W. Gu, P. Cheng, M. Tang, *R. Soc. Open Sci*. **2018,** *5*, 171936.

[34] R. C. Alkire, H. Gerischer, D. M.Kolb and C. W. Tobias (Eds.), Advanced in Electrochemical Science and Engineering, Vol.5, Wiley-VCH, **1997,** Weinheim, Germany.
[35] C. Wagner, *J. Electrochem. Soc.* **1951,** *98*, 116-128.
[36] Z. Wang, S. Sankarasubramanian, V. Ramani, *Cell Rep. Phys. Sci.* **2020,** *1*, 1-15.
[37] Z. Niu, R. Wang, K. Jiao, Q. Du, Y. Yin, *Sci. Bull.* **2017,** *62*, 31-39.
[38] J.J. Hwang, C.H. Chao, W. Wu, *J. Power Sources* **2006**, *163*, 450–459.